Experimental Characterization of SPT-100 Hall Effect Thruster Operating in a Pulsed Mode

IEPC-2024-137

Presented at the 38th International Electric Propulsion Conference, Toulouse, France
June 23-28, 2024

Lubos Brieda*
Particle in Cell Consulting LLC, Westlake Village, CA 91362, USA

This papers presents results from an experimental characterization of the SPT-100 Hall Effect Thruster operating in a pulsed mode with Krypton used as the propellant. Such an operation has been proposed as a method for testing high powered Hall thruster in facilities lacking the needed pumping capacity. After initial conditioning, the thruster is pulsed between nominal and reduced anode flow rate mode. Relevant properties of interest, such as thrust or plume plasma densities, are recorded in the short time period before chamber pressure becomes too large. The objective of this test was to experimentally determine if such an approach is indeed feasible. The experiment utilized high speed data acquisition to sample the discharge current in order to characterize the length of the transition period. Additional telemetry was provided by an externally mounted camera, thermocouples, pressure gauges, flow meters, inverted pendulum thrust stand, Langmuir and retarding potential analyzer (RPA) probes, as well as a residual gas analyzer (RGA). We find that this particular device can indeed be operated in a pulsed mode, with discharge current and thrust returning to within 85% of their nominal values on time scales shorter or equal to the pressure increase time.

I. Introduction

Hall Effect Thrusters (HETs) are spacecraft propulsion devices that produce thrust by ionizing and accelerating the propellant gas in an open channel configuration. While the majority of HETs used for station keeping operate at power levels of several kilowatts, higher powered devices have been identified as enabling technologies for a number of deep space exploration and space tug missions.[1–4] Testing of high powered Hall thrusters remains challenging due to the limitations in vacuum chamber pumping speeds. There are only a handful facilities world-wide that contain adequate pumping capacity to maintain a sufficiently low pressure (generally assumed as 10^{-5} Torr or below[5]) with propellant flow rates associated with the 100 kW-plus power levels. To the best of our knowledge, no facilities exist *at all* that are capable of supporting testing at the mega watt level. For this reason, in[6] the authors proposed a method for testing Hall thrusters in a quasi-steady pulsed mode, in which the anode flow is cycled between the nominal and a reduced rate. The purpose of the low-flow mode is to allow the pumps to "catch up" and temporary reduce the pressure. Operational and environmental conditions, such as thrust, mean discharge current, or the near field plasma density and potential are then recorded in the short interval after the flow rate is restored to the nominal value before the chamber pressure becomes excessively large. To minimize the number of transient factors, all other thruster operating conditions, such as discharge voltage, magnet current, and propellant flow through the cathode, remain in their nominal state. The prior work in[6] was based on a numerical analysis of the SPT-100 Hall thruster with the industry standard simulation tool HPHall.[7] These simulations indicated that the thruster is indeed capable of running in a pulsed mode, with the discharge transitioning into a glow mode during the low mass flow rate operations. The transition back to the nominal state was essentially instantaneous once the full anode flow was restored. Such a rapid transition is not realistic in practice, since the real-world system is affected by additional external factors, such as the cooling of the discharge channel walls, that are not captured by the numerical model.

*President, lubos.brieda@particleincell.com

This paper builds on this past numerical study by exploring this quasi-steady concept experimentally. Specifically, we use the SPT-100 Hall Effect Thruster running on krypton to first confirm that this pulsed operation is indeed possible, and second, to characterize the time required for parameters of interest to transition to the nominal condition once the full anode flow anode rate is re-established. This 1.35 kW thruster is used in lieu of a high power device for practical reasons as a larger thruster would require a larger – and hence more expensive – chamber to operate. While the start up behavior of a Hall thruster has been studied experimentally by other researchers,[8–10] the only past published experimental work focusing on the dynamics of the start up behavior of a pre-conditioned thruster seems to be a 2001 report of Hruby, et.al.[11] In that report, the authors focused on repeated restarts of a powered off thruster, and found the longest transient time to be associated with the diffusion of the magnetic field through the discharge. This transient is not expected to be a factor during the quasi-steady operation of a typical Hall thruster since neither the discharge nor the magnetic field are extinguished. We begin the paper by describing our experimental setup. We then present the initial set of characteristics from a pathfinder test, in which we demonstrate that this device can indeed be run in a pulsed mode. We subsequently dive into the characterization of the transitions by collecting high frequency discharge current telemetry over a one minute interval. We also characterize the impact of pulsing on the thrust and on the near-field plume properties and ion energies, and conclude the paper by summarizing the observed transition times.

II. Experimental Setup

A. Vacuum Facility

The study was performed in Chamber 1 at the Air Force Research Laboratory (AFRL) at Edwards Air Force Base, California, USA. Chamber 1 is a cylindrical, stainless steel vacuum chamber measuring 2.4 m in diameter and 4.1 m in length. The side walls and ceiling are covered with low sulfur graphite of 1.8 mm thickness.[12] Both chamber end caps house graphite beam dumps to reduce redeposition of sputtered materials. Pumping was provided by two liquid nitrogen-baffled, gaseous helium two-stage cryogenic vacuum pumps. Under these conditions, the chamber pressure was measured to be 1.8×10^{-5} Torr at nominal conditions using krypton at 65.4 sccm propellant flow rate. A cold cathode gauge located on the same plane as the thruster was used to monitor chamber pressure throughout testing. All pressures reported in this paper have been corrected for krypton. The thruster was placed in the vacuum chamber and allowed to outgas for at least 12 hours at pressures below 1×10^{-4} Torr before testing began. An SRS RGA 300 rarefied gas analyzer (RGA) was attached to the side of the chamber ∼254 mm in front of the thruster exit plane to track the gas composition within the chamber. The thruster was also instrumented with thermocouples. Plasma probes, as described below, were placed on a stationary probe in the near-field region. An image of the experimental setup is shown in Figure 1 and a schematic is found in Figure 2.

B. Thruster

A flight model SPT-100 Hall effect thruster with a conventional five-core magnetic circuit was used in this study. The acceleration channel of the thruster was measured at 100 mm outer diameter and 50 mm inner diameter. Discharge current is routed through the magnetic circuit and thus the magnetic field cannot be controlled independently from the anode current. The thruster is equipped with two lanthanum hexaboride (LaB_6) cathodes, although only one cathode was used during this study. Using krypton, the thruster is characterized as having 63 mN of thrust under nominal operating conditions. The thruster and cathode were operated using server-rack-mounted Sorensen power supplies controlled by LabVIEW software while the krypton was supplied to the thruster using two FC-PAR7800C digital mass flow controllers from Aera.

C. Thrust Stand

An inverted pendulum design thrust stand was used in this study, similar to that designed by Haag at NASA Glenn Research Center.[13] The displacement was calculated using an optical sensor that measures the distance from a mirror to the fiber optic cable. The zero-point of the pendulum was maintained by applying finite current to a null coil to generate a restoring force on the pendulum arm to counteract translation due to thrust. This electromagnetic force is generated by a feedback system using a proportional-integral-derivative (PID) controller to ensure stable operation. Under the assumption of a linearly proportional restoring force,

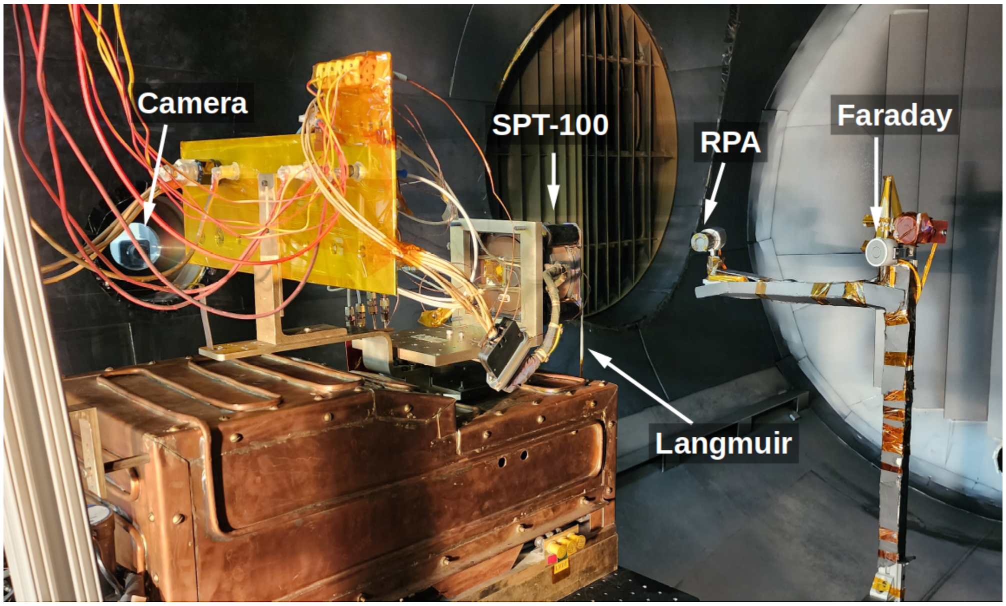

Figure 1: Photograph of the experimental instrumentation.

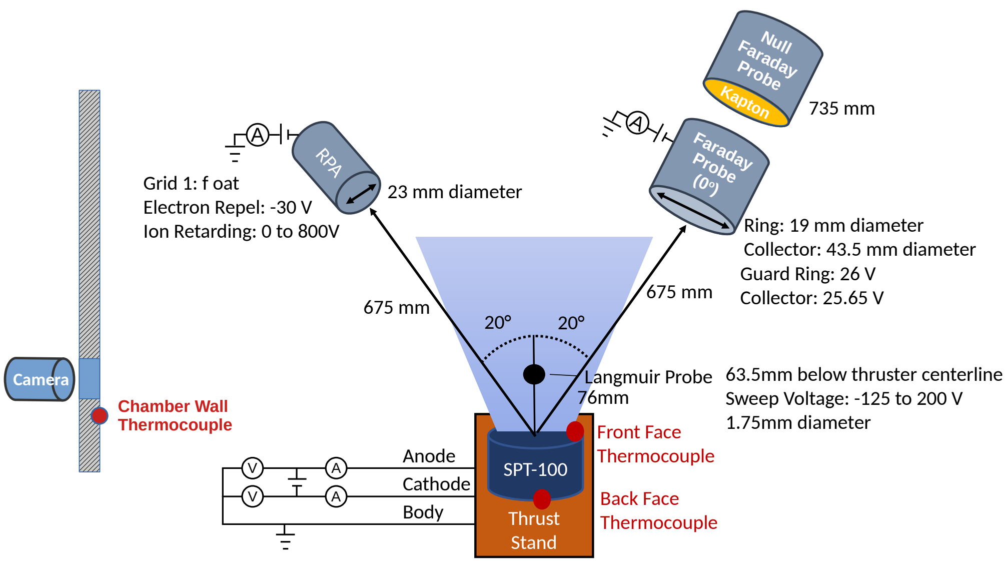

Figure 2: Experimental setup schematic.

the thrust stand was calibrated using a series of mechanical weights being loaded and unloaded from the system to correlate null coil voltage to known restoring forces. To prevent large changes in thrust stand temperature during thruster operation, chilled ethylene glycol was flowed through the shroud of the thrust stand. Thermocouples placed on the thrust stand shroud as well as the null coil cooling plate were used to track the thermal drift of the components throughout testing. Before and after each series of pulsing tests, a calibration of the thrust stand was performed using the mechanical weight loading system to generate a new calibration curve. The thrust calculations based on the null coil current are performed during post-processing, using the appropriate calibration slopes and offsets depending on the time of day of a given test.

D. Faraday Probe

The ion current flux was measured using a guarded Faraday probe. Ion current was collected on a disk measuring 19 mm in diameter while a concentric guard piece measuring 43.6mm in outer diameter was used to minimize the effects of the plasma sheath on the collection area. A 1 mm wide gap existed between the collector and guard ring. The effective current collector area was assumed to consist solely of the collector front plate as qualitative results are the main interest in this study. The collector and guard ring were biased to -25 V and -30 V, respectively, with respect to chamber ground to achieve ion saturation. The collector is biased using a series of 12 V batteries while the guard ring was powered using a TDK Lambda power supply. The returning current was measured by a transimpedance amplifier. Secondary electron emission effects were assumed negligible for the analysis in this paper. The Faraday probe was placed along the vertical thruster centerline, 20 deg off axis of the thruster face. The distance from Faraday probe face to thruster exit plane was measured to be 675 mm. A null probe was placed directly behind the faraday probe at 735 mm from the thruster exit plane, and a half-thruster diameter above the first Faraday probe to calculate some amount of noise to be subtracted from the biased Faraday probe results. Note that only the collector of the null probe is biased to -25 V; the guard ring was left unattached.

E. Retarding Potential Analyzer

The retarding potential analyzer (RPA) used in this experiment was a four-grid design. RPA is effectively an energy-filtered Faraday probe, and these grids are used to screen different components of the incident plasma population. The first grid acts as an aperture to constrict the plasma flow to the probe and is allowed to float at the local plasma potential. The second grid is used to suppress electrons with a -30 V bias provided by a TDK Lambda power supply while still allowing ions to pass through. The third grid is the ion retarding grid which is swept positively over a few hundred volts relative to chamber ground to allow selective passage of ions based on their kinetic energy using a Keithley 2410 SourceMeter. The final grid is measured by a Keithley 6485 Picoammeter to create the resulting energy distribution plot. The probe returns a current reading which can be used to calculate the derivative of the current per unit area as

$$d\Gamma/dV_0 = qe/mf(V) \tag{1}$$

which is proportional to the ion energy-per-charge distribution of the plasma, $f(V)$.[14] The RPA was placed along the vertical thruster centerline at 20 deg off the horizontal centerline, directly opposite the Faraday probe and 675 mm from the thruster exit plane. The probe was shrouded in graphite to prevent any sputtering or charge build-up on the device. The effective grid area used to calculate results was based on a 23mm diameter circular aperture.

F. Langmuir Probe

A single tip, shrouded, planar Langmuir probe was used to sample the plasma current-voltage I-V curve from which it is possible to determine various plasma characteristics such as density, temperature, and potential. This probe is a biased conductor placed inside a plasma to induce electron and ion currents on the probe that can be measured. The probe was placed 63.5 mm below the thruster centerline and 76 mm from the exit plane, perpendicular to the ion velocity direction in the very near-field region of the plume.[15] In this region, the probe was anticipated to be small enough to not disrupt the plasma appreciably. Post-processing of the data indicates that the Langmuir tip may have still been too small for this location, but the results showed the desired trends sufficiently that the tests were not attempted to be redone due to time constraints. The effective radius of the tip is 1.75 mm. The potential bias was swept from -125 V to 200 V using a Keithley 2410 SourceMeter to systematically attract both ions and electrons and determine their respective saturation potentials as required to extract plasma characteristics.

G. Data Acquisition

Data was acquired using a NI PXIe-1084 data acquisition (DAQ) system as well as a LeCroy 8-channel HD0-8108A high speed oscilloscope. The thruster operating inputs including power supply outputs, mass flow control rates, and operating power were both controlled and sampled at a 0.3 Hz rate. All Faraday probe diagnostics as well as anode and cathode voltages and currents were sampled at either a 25 MHz for 0.1 s or 500 kHz for 200 s of continuous data. The thrust data was taken at 2.5 kHz for both acquisition time scales. The 200 s continuous data captured the full transition of the thruster during the increase or decrease in anode mass flow rate while the 0.1 s data was taken over a 10-15 min time scale to study the longer settling time of the plasma. Temperature was sampled once every 10 s to track the thermal stability of the thruster. The RPA and Langmuir probes were continuously swept by LabVIEW, taking a few seconds each to complete a single sweep.

H. Video Feed

Video footage of the thruster plume was taken using a SONY SNC-VB630 camera that has recording capabilities up to 60 frames per second and a resolution of 1080p. Camera exposure, sharpness, and contrast were optimized to refine the near-field plasma plume as much as possible. The camera was positioned perpendicular to the thruster exit face on the same plane, peering into the chamber from a viewport. Lighting from outside the chamber was blocked using a black shroud over the camera and viewport.

III. Pathfinder Test

A. Test Sequence

The testing campaign was initially conducted from January 30th to February 1st, 2023, with these days referred to as Day 1, Day 2, and Day 3. Day 1 was used to install the equipment. The chamber door was closed in the afternoon, and the chamber was left to pump overnight. The first set of cycling operation was conducted during Day 2. During this phase, it was discovered that that high speed data acquisition was limited to collecting only approximately 10 seconds of data, as longer sampling periods led to a crash of the LabVIEW software. The afternoon session was then used to diagnose this issue, which involved adjusting buffer sizes and reducing sampling frequency on the oscilloscope. High frequency measurements of the thruster discharge current during the transitions were then obtained during Day 3. We also used this day to sample the plume and thrust dynamics. However, subsequent data analysis indicated that a possible wiring issue made these measurements unusable. The chamber was subsequently repressurized to address these connectivity issues. An additional tests were then conducted February 7th (Day 4) and February 23rd (Day 5). In all cases, the chamber was left to pump overnight before testing was initiated. These two dates were used to obtain thrust measurements (Day 4) and Langmuir probe readings (Day 5).

B. Initial Pulsing Test

Figure 3 plots telemetry from the pulsing characterization on Day 2. The horizontal axis corresponds to the time elapsed since the data acquisitions start at 7:43 am. The first half hour involved tests of the mass flow controllers. The power supply was then activated to provide 300 V of potential difference between the cathode and the anode. This setting, indicated by the dashed red line, remained fixed for the duration of the test. The only observed deviation in supplied voltage corresponds to a temporary drop upon the initial ignition, as can be seen around minute 35. This event is also accompanied by a spike in pressure shown by the black trace. The spike could be arising from a flash-off of surface adhered contaminants and water vapor. The green dashed line plots the average discharge current. The thruster was left to operate for 85 minutes to establish the baseline nominal state. We then conducted several pulsing tests by commanding the flow controller to reduce the anode flow rate to 30% of the nominal value. This reduction was selected based on the prior experience with this thruster, as lower flow rates were found to lead to an instability and an extinction of the discharge. The cathode flow, shown by the light blue dash-dotted line, remained constant. The reduction in the anode flow leads to an almost immediate drop of the discharge current from the nominal 4.45 A to 0.59 A. We do not observe any impact on the discharge voltage, which remains fixed by the power supply at 300 V. Pressure is also seen to drop in line with the mass flow rate reduction from 1.86×10^{-5} to 6.78×10^{-6} Torr.

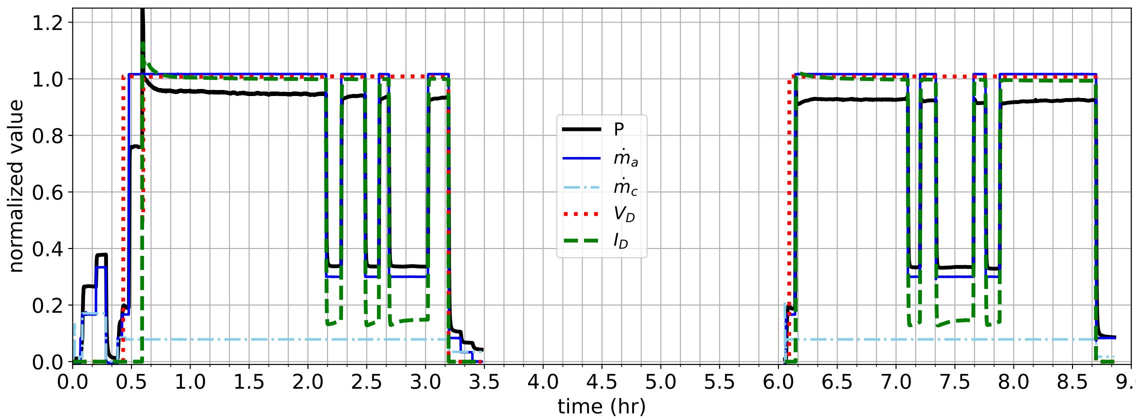

Figure 3: Day 2 test sequence. Values are normalized by $p_0 = 2 \times 10^{-5}$ Torr, $\dot{m}_0 = 60$ ccms, $V_0 = 300$ V, and $I_0 = 4.45$ A.

C. Discharge Current Frequency Spectrum

Figure 4 plots the discharge current power density spectrum as computed using the Welch filter with a 40,000-item window as implemented in NumPy. This plot corresponds to the afternoon session in Figure 3. The source data was obtained by concatenating a sequence of 610 files, each capturing 10 seconds of data samples at 1 Mhz frequency. Each horizontal plot line corresponds to an instant in time, with time increasing from bottom to top. Horizontal grid lines denote 3 minute intervals. We can see that it takes the discharge approximately 3 minutes to reach a steady state after the initial power on. This nominal operation is characterized by the breathing mode at 17 kHz and another weaker mode at 33 kHz. The breathing mode frequency is in a generally good agreement with literature.[16] Higher modes are not visible, but this could be a limitation of the sampling frequency. At the 7.1 hour mark we see the first transition to the low flow mode. The breathing mode completely disappears, and instead we observe a broad mode centered on 7 kHz. Approximately at the 7.2 hour mark, the thruster is transitioned to the nominal mode. The discharge current oscillations return to the nominal breathing mode dominated state almost instantaneously.

D. Plume Images

The reduction in the anode flow also led to noticeable change in the plume shape. Figure 5 shows snapshots from the video camera feed corresponding to the pulsing commencing at time 2.485 hrs (149.1 minutes) in Figure 3. The behavior seen here was typical of all cycles. The reported time indicates the time difference from the start of the transition to the low flow mode. The first image shows the typical thruster plume during the nominal operation. The plume has a blueish tint, and features a well defined central jet. A wing structure extends to a distance of around a thruster radius. The near plume region is further dominated by a bright white glow. Six seconds after the flow reduction, the plume still retains these features, but their intensity has been reduced. The plume also begins to take on a pinkish hue. At 16 seconds, the central jet is still visible but the previously narrowly confined wing structure begins to expand axially. By 1:16, the plume transitions to a glow mode defined by an isotropic expansion and absence of the central jet. This profile remains for the duration of the low flow mode, as can also be seen by comparing to the 5:16 snapshot. The transition back to the nominal flow begins at time 7:00. Almost immediately, we can observe a faint sign of the central jet region. 11 seconds after the transition began, the plume color begins to revert back to the blueish tint and the glow region starts collapsing back towards the exit plane. The plume brightness

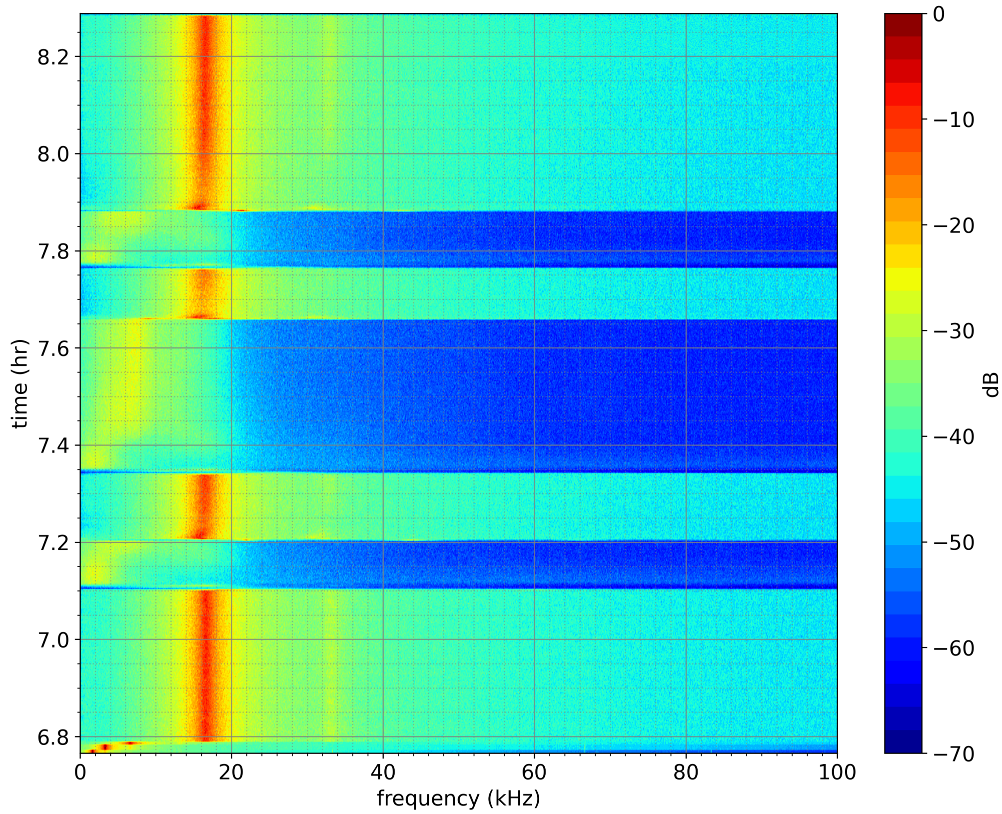

Figure 4: Discharge current frequency spectrum for Day 2 testing.

continues to increase, and by 7:21, the plume achieves the profile corresponding to the nominal operation. It remains in this state for the entirety of the nominal flow rate.

E. Chamber Environment

Figure 6 shows a time history plot of the chamber environment mass composition as sampled by the SRS RGA over a 24 hour period starting with the initial pump down at 4:41 pm on Day 1. The RGA was left in a continuous sampling mode with every 10th trace written out to the log file. The plot was then generated by parsing the produced .ana binary files using a custom Python script. The RGA was scanning up to atomic mass unit (amu) 200, however, no species heavier than Krypton (84 amu) were observed. The colormap plots the base 10 logarithm of the species partial pressures. We can clearly observe the slow depletion of water indicated by the fragments centered around 18 amu. After four hours on vacuum, water vapor concentration has decreased by only 0.7 orders of magnitude. After 12 hours, the reduction is still only 1.48 orders of magnitude. After 16 hours, which corresponds to the initial pulsing pathfinder experiment, the reduction reaches two orders of magnitude. It then continues a slow decay, reaching $10^{2.38}$ reduction by hour 48. Gradual decay is also observed in the nitrogen (28 amu) and oxygen (32 amu) lines. The source of the pressure spike around hour two is not clear. Just prior to the start of the first pulsing test, water vapor concentration is $4.3\times$ and $8.3\times$ higher than the concentration of molecular nitrogen and oxygen, respectively. Water is thus seen to be the primary constituent of the chamber environment whenever krypton is not flowing. As such, some of the start up transient behavior historically observed by other researchers may be attributable to water contamination. The interval between hours 18 and 21 corresponds to a lunch break and a subsequent work on the diagnostic system during which the thruster was switched off. We can clearly see that propellant is easily removed by the pumps as there is no lingering krypton trace once the flow is stopped. The reduction in the krypton concentration corresponding to the pulsed operation is also easily seen at the 23 hour mark.

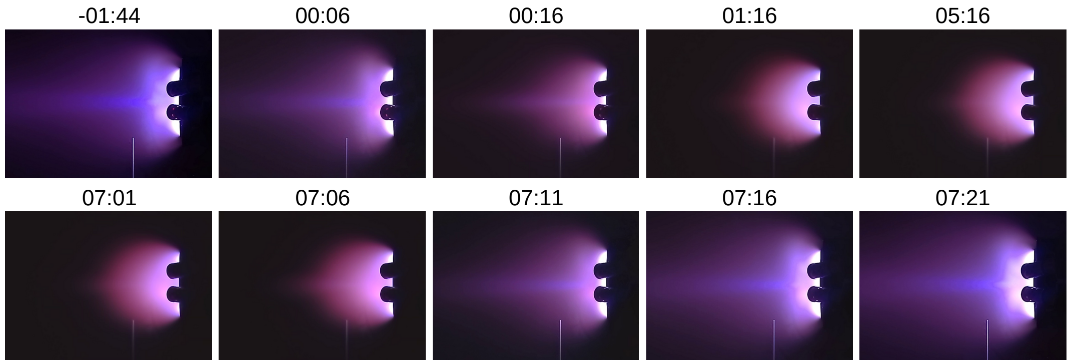

Figure 5: Illustration of typical plume variation during a pulse, with time in minutes and seconds. Transition from nominal to reduced flow begins at time 0. Return to nominal flow begins at minute 7.

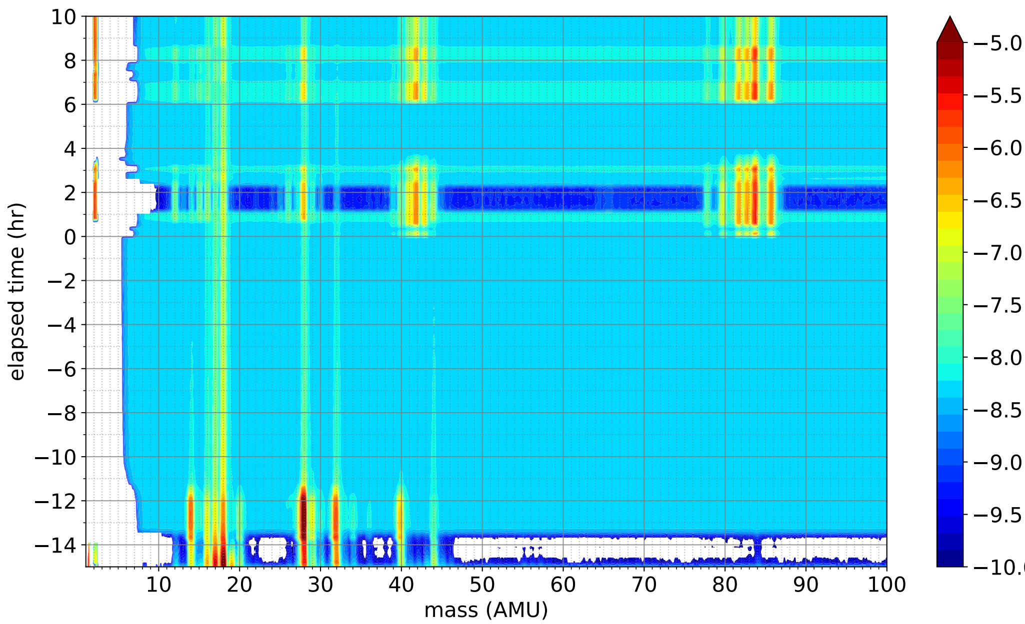

Figure 6: Evolution of the RGA mass spectrum from the initial pump down to the first set of cycling tests. Time offset is computed from the start of Day 2 testing. Colors correspond to $\log_{10}$ of the partial pressures.

IV. Pulsed Mode Dynamics

A. Discharge Current

The majority of effort during the second half of Day 2 involved modifying the settings for the data acquisition system to support sampling of high frequency data over a sufficiently long period to capture the transition between the nominal and reduced flow rate modes. The chamber was left under vacuum overnight. Day 3 testing then involved collecting high frequency telemetry of discharge current during two sets of pulses. 60 seconds of telemetry was collected at 500 kHz with an approximately 10 second lead time prior to the start of each transition. Plots of the discharge current and the corresponding power spectrum can be seen in Figure 7. Plots (a) and (c) visualize the transition from nominal to low flow mode, while plots (b) and (d) show the return to nominal. In both cases, the time axis is centered on the transition start time. We can observe that the mean discharge current begins to decay as soon as the flow is reduced. However the breathing mode remains present for approximately 12 seconds. This telemetry agrees with the visual observation in Figure 5, in which we can see the central core greatly reduced by the 16 second mark. Over the next 28 seconds, the current gradually evolves to the broad spectrum centered on 4 kHz , as was observed in the discrete data in Figure 4.

The transition to the nominal mode in Figure 7 (b) and (d) is of interest to high power Hall thruster testing. A dominant breathing mode signal first appears at 3 seconds, however the next five seconds involve the device searching for a stable state. Between seconds 12 and 16, we can observe the appearance of a secondary mode at 32 kHz, and a yet another weaker mode at 50 kHz. These modes then disappear, only for the 32 kHz signal to reappear in a weaker form 24 seconds post transition. From figure (b), we can see that it takes 20 seconds for the mean discharge current to the return to the nominal state.

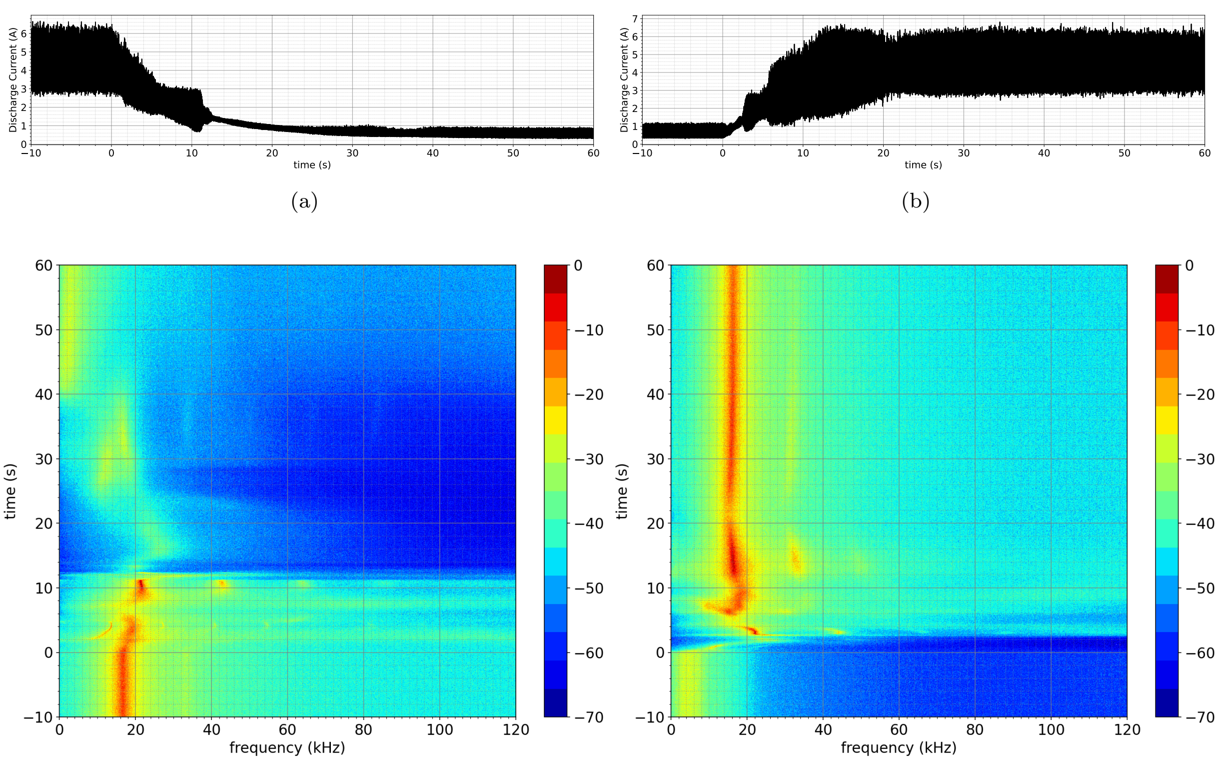

Figure 7: Discharge current and power spectrum density for transition from nominal to low flow mode (a) and (c), and transition to nominal operation (b) and (d).

B. Thrust and Temperature

Figure 8 visualizes the impact of the pulsed operation on thrust and temperature. The gray trace plots the normalized thrust, while the dashed red line correspond to the read out from a thermocouple mounted to the thruster body. The black trace corresponds to the chamber pressure, while the green dashed line shows the anode mass flow rate. While the pulsed operation has a clear impact on the thruster temperature, the temperature variation is not seen to have any observable impact on thrust. This is an important finding since the lack of thermal stability was previously cited as one of the drawbacks of the pulsed operation. From the figure, we can also conclude that thrust recovers on time scales shorter, or at least comparable to the pressure rise. By zooming in on the final transition around minute 43.5, we can observe that anode flow increase from the reduced rate to the baseline rate takes approximately 10.32 seconds. The corresponding pressure increase requires 28.26 seconds. Thrust transition to the nominal level requires 19.68 seconds, however an 85% level is reached is 10.26 seconds.

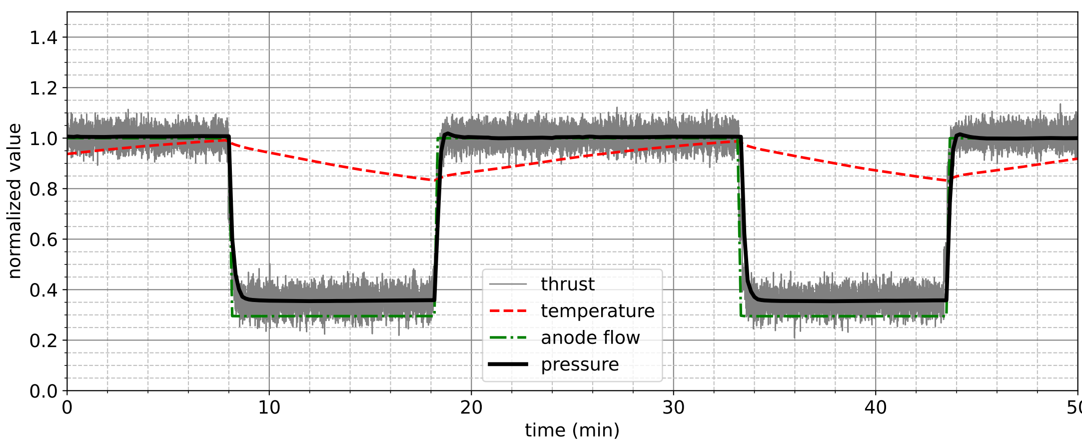

Figure 8: Temporal variation in thrust, chamber pressure, and thruster temperature. Values are normalized by $T_0 = 215$ mN, $p_0 = 1.81 \times 10^{-5}$ Torr, and $Q_0 = 61$ sccm.

C. Plume Properties

Figure 9 plots the temporal variation from the Langmuir probe obtained by following the analysis method from.[15] This particular data set comes from Day 5 testing since the data obtained during the nominal day 3 testing was found to be corrupted due to probe grounding issues. However, even despite the corrective actions taken, the Langmuir data was found to be of limited use. Specifically, electron temperature and plasma potential signal was saturated by noise making it impossible to extract a clear signal trace. Electron and ion densities, as well as the floating potential were found to respond on time scales comparable to the mass flow rate variation. The Langmuir probe was also run in an ion saturation mode in which the probe voltage was fixed at -25 V and probe current was measured every 5 seconds. Measurements from this mode are shown by the purple line. We observe the current to follow the anode flow rate as well as the pressure trend in Figure 8. In under 11 s, the current reaches the steady value and subsequently overshoots its by approximately 5%. The current then slowly decays to the nominal state over the next two minutes.

Figure 10 plots the temporal evolution of the ion energy spectrum over two pulses. This data was obtained by differentiating the cumulative current from an RPA sweep. The data was sampled at 60 seconds intervals per sweep and as such, does not provide the high resolution response of the prior plots. Given this limited data resolution, we observe an essentially instantaneous transition to the nominal energy profile upon the restoration of the full anode flow.

D. Settling Times

The prior sections characterized the temporal variation from several different sensors. Settling times, defined to mean the time required for a property to return to 85% of the nominal value, for the previously discussed

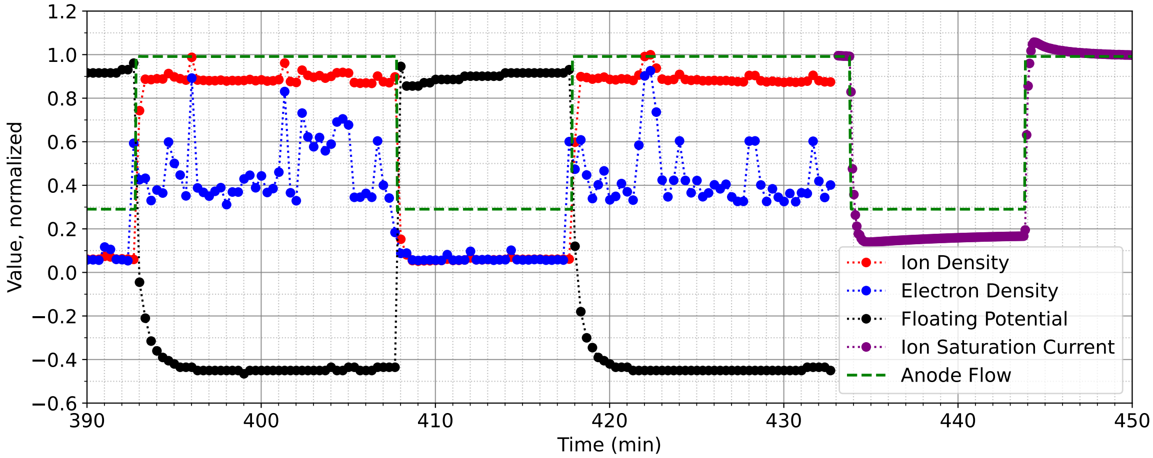

Figure 9: Temporal response in plume properties as measured by the Langmuir probe.

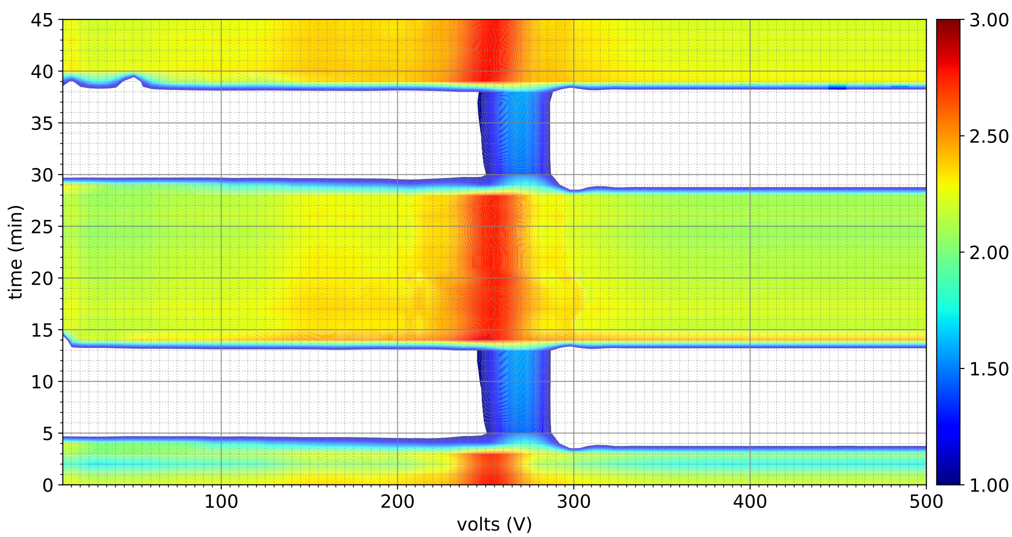

Figure 10: Ion energy spectrum from the RPA probe.

diagnostics, are summarized in Table 1.

property	settling time
discharge current	5 s
thrust	10.26 s
pressure	28.26 s
ion saturation current	11 s
ion energy spectrum	$\leq$ 1 min

Table 1: Summary of settling times

V. Conclusion

This paper introduced data from an experimental characterization of the SPT-100 Hall thruster operating in a pulsed mode in which the anode flow rate was cycled between the nominal and a reduced flow phases. Specifically, our interest was in determining the duration needed for the thruster to return to the nominal mode after the full flow mode was re-established. We find that the thruster can be operated in this cycled mode, with stable operation observed down to a 30% reduction in the anode mass flow rate. We also observed that properties of interest, such as thrust, discharge current, and near field plume plasma characteristics return to 85% of their nominal state within approximately 10 seconds. The pressure increase time was observed to be 28 seconds, indicating that it is indeed feasible to use a pulsing mode to perform rapid measurements of thruster operating conditions.

Acknowledgements

The author would like to thank Dr. Christine Greve and Cameron Marsh from the Air Force Research Laboratory for aiding in the collection of data used in this study. The views expressed in this document are those of the authors and do not reflect official policy or position of the United States Air Force, Department of Defense, or the United States Government.

References

[1] Roland Florenz, Thomas Liu, Alec Gallimore, Hani Kamhawi, Daniel Brown, Richard Hofer, and James Polk. Electric propulsion of a different class: The cHallenges of testing for megawatt missions. In *48th AIAA/ASME/SAE/ASEE Joint Propulsion Conference & Exhibit*, 2012.

[2] Sarah E Cusson, Marcel P Georgin, Horatiu C Dragnea, Ethan T Dale, Vira Dhaliwal, Iain D Boyd, and Alec D Gallimore. On channel interactions in nested Hall thrusters. *Journal of Applied Physics*, 123(13):133303, 2018.

[3] Ronald Spores, Jeff Monheiser, Brian P Dempsey, Darren Wade, Kenneth Creel, David Jacobson, and Geoff Drummond. A solar electric propulsion cargo vehicle to support NASA lunar exploration program. In *IEPC Paper No. IEPC-2005-320, 25th International Electric Propulsion Conference, Princeton, NJ, October*, volume 31, 2005.

[4] Nathan Strange, Raymond Merrill, Damon Landau, Bret Drake, John Brophy, and Richard Hofer. Human missions to phobos and deimos using combined chemical and solar electric propulsion. In *47th AIAA/ASME/SAE/ASEE Joint Propulsion Conference & Exhibit*, page 5663, 2011.

[5] T Randolph, V Kim, H Kaufman, K Kozubsky, VV Zhurin, and M Day. Facility effects on stationary plasma thruster testing. In *23rd International Electric Propulsion Conference*, pages 13–16, 1993.

[6] Lubos Brieda, Yevgeny Raitses, Edgar Choueiri, Roger Myers, and Michael Keidar. Quasi-steady testing approach for high-power hall thrusters. *Journal of Applied Physics*, 130(18), 2021.

[7] John M. Fife. *Hybrid-PIC Modeling and Electrostatic Probe Survey of Hall Thrusters*. PhD thesis, Massachusetts Institute of Technology, 1998.

[8] William A Hargus and Bruce Pote. Examination of a Hall thruster start transient. In *38th AIAA/ASME/SAE/ASEE Joint Propulsion Conference & Exhibit*, page 3956, 2002.

[9] F Taccogna, S Longo, M Capitelli, and R Schneider. Start-up transient in a hall thruster. *Contributions to Plasma Physics*, 46(10):781–786, 2006.

[10] R Santos, E Ahedo, Y Raitses, and NJ Fisch. Transitional regime in the start-up process of conventional Hall thrusters. In *32nd International Electric Propulsion Conference (IEPC)*, 2011.

[11] Vlad Hruby, Bruce Pote, Manuel Gamero-Castaño, George Kolencik, Larry Byrne, Rachel Tedrake, and Mary Delichatsios.

Hall thrusters operating in pulsed mode. In *27th International Electric Propulsion Conference, Pasadena, California*, pages 01–66, 2001.

[12]Michael Nakles, William Hargus, Jorge Delgado, and Ron Corey. A performance and plume comparison of xenon and krypton propellant on the SPT-100. In *48th AIAA/ASME/SAE/ASEE Joint Propulsion Conference & Exhibit*, Atlanta, GA, 2012.

[13]T.W. Haag and F.M. Curran. Arcjet starting reliability: A multistart test on hydrogen/nitrogen mixtures. Nasa technical memorandum 89867, Lewis Research Center.

[14]I. Hutchinson. *Principles of Plasma Diagnostics*. Cambridge University Press, 1994.

[15]Robert Lobbia and Brian Beal. Recommended practice for use of langmuir probes in electric propulsion testing. *Journal of Propulsion of Power*, 33(3), 2017.

[16]Natalia MacDonald-Tenenbaum, Quinn Pratt, Michael Nakles, Nickolas Pilgram, Michael Holmes, and William Hargus Jr. Background pressure effects on ion velocity distributions in an SPT-100 Hall thruster. *Journal of Propulsion and Power*, 35(2):403–412, 2019.